

Article

A Novel Nanogold Composite Fabrication, Its Characterization, and Its Application in the Removal of Methylene Blue Dye from an Aqueous Solution

Einass A. Abood¹, Wafa K. Essa^{2,*}, Ali Alsuraifi³ and Suhad A. Yasin^{2,*}¹ Polymer Research Center, University of Basrah, Basrah 61004, Iraq; einas.abood@uobasrah.edu.iq² College of Science, University of Duhok, Duhok 42001, Iraq³ College of Dentistry, University of Basrah, Basrah 61004, Iraq; ali.yassen@uobasrah.edu.iq

* Correspondence: wafa.k.essa@uod.ac (W.K.E.); suhad.yasin@uod.ac (S.A.Y.)

Abstract: A unique aspect of this research lies in the combination of polyethylene terephthalate (PET) nanofibers with Au⁰@PPh₂-PILP to create a nanogold composite (NGC). This NGC has proven to be highly efficient in removing methylene blue (MB) from wastewater. The prepared nanogold composite NGC was characterized by Fourier-transform infrared spectroscopy (FTIR), Field Emission Scanning Electron Microscopy (FE-SEM), transmission electron microscopy (TEM), Energy Dispersive X-ray Spectroscopy (EDAX), and Elements Distribution Mapping (EDM). Several factors were examined in batch adsorption experiments to determine their impact on dye adsorption. These factors included the initial pH range of four to eight, the dosage of NGC adsorbent ranging from 0.001 to 0.008 g, the initial concentration of MB dye ranging from 10 to 50 mg L⁻¹, and the contact period ranging from 10 to 80 min. It has been observed that NGC is more efficient in removing MB from polluted water. The results of the pseudo-second-order model show good agreement between the calculated adsorption capacity (q_e)_{cal.} (4.3840 mg g⁻¹) and the experimental adsorption capacity (q_e)_{exp.} (4.6838 mg g⁻¹) values. Experimental findings suggest a monolayer capping of MB dye on the NGC surface with a maximum adsorption capacity Q_m of 18.622 mg g⁻¹ at 20 °C, indicating that it is well-fitted to the Langmuir isotherm.

Keywords: polyethylene terephthalate; nanofiber; nanogold; methylene blue; nanocomposite

Citation: Abood, E.A.; Essa, W.K.; Alsuraifi, A.; Yasin, S.A. A Novel Nanogold Composite Fabrication, Its Characterization, and Its Application in the Removal of Methylene Blue Dye from an Aqueous Solution. *Appl. Sci.* **2024**, *14*, 5229. <https://doi.org/10.3390/app14125229>

Academic Editor: Ntaote David Shooto

Received: 20 May 2024

Revised: 4 June 2024

Accepted: 5 June 2024

Published: 17 June 2024



Copyright: © 2024 by the authors. Licensee MDPI, Basel, Switzerland. This article is an open access article distributed under the terms and conditions of the Creative Commons Attribution (CC BY) license (<https://creativecommons.org/licenses/by/4.0/>).

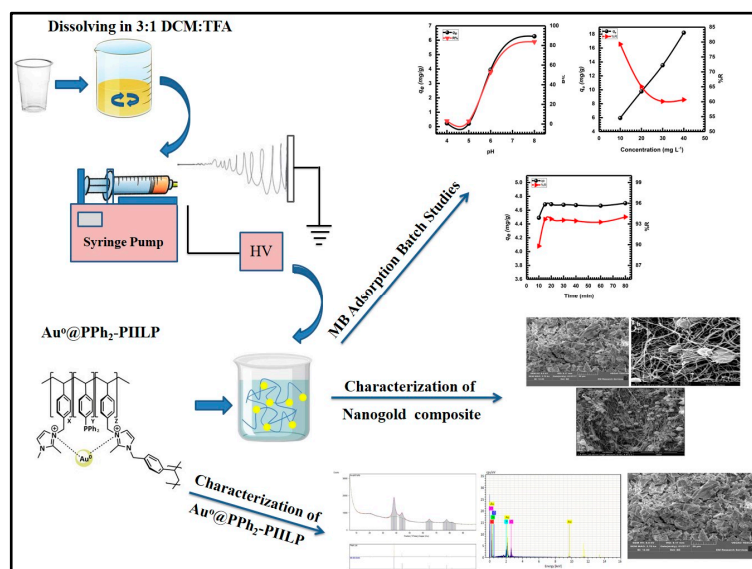
1. Introduction

Over the last decades, water pollution has emerged as a significant global challenge, posing a crucial threat to both the planet and human well-being as a result of increased industrialization activity around the world and attendant discharges of toxic substances directly into water sources without any treatment, which have led to a decrease in the amount of water suitable for human consumption [1,2]. A report released by UN-Water anticipated that by 2025 approximately two-thirds of the global population will experience water stress. The report further projected that approximately 1.8 billion individuals would experience absolute water scarcity in their living conditions [3]. Thus, wastewater treatment has become crucial for a sustainable existence. Many techniques have been used for this purpose, including photodegradation [4,5], adsorption [6,7], distillation [8,9], electrolysis [10,11], and membranes [12,13]. Adsorption is the most commonly used method for treating dye-containing wastewater dyeing wastewater due to its simple operation, low cost, and effectiveness, according to the literature [14]. Adsorbents such as zeolites, activated carbon (AC), polymers, and biomaterials have long been utilized in traditional wastewater treatment processes. However, these materials have a limited adsorption efficiency. Finding more effective adsorbents has therefore become crucial [15,16]. Based on the literature, it is evident that the incorporation of nanomaterials in membranes has shown a remarkable improvement in their properties, such as water permeability, mechanical strength, and separation efficiency, in addition to reducing fouling of

the membrane [17–19]. Polymer nanofibers have been explored in recent years as one of the most promising materials for water treatment membranes due to their unique physicochemical properties, such as nanoscale size, high surface area, and large porosity [20]. In this regard, an electrospinning technique has been used to generate nanofibers from various types of polymers. Moreover, by introducing nanomaterials as additives into polymer nanofiber membranes, the prepared nanocomposite membrane can possess additional features [21]. The eventual composites are expected to have a huge potential to purify water. This perhaps is due to their cost-effectiveness, high chemical reactivity, and surface area, in addition to excellent mechanical strength [22]. The present research involves repurposing PET cups for the production of PET nanofibers through electrospinning. Despite their prior use, their efficiency was lacking. Consequently, a concept emerged to merge them with gold nanoparticles to enhance their efficacy and optimize their performance in eliminating methylene molecules. This process aims to eliminate PET and methylene waste, thereby contributing to environmental improvement. There have been reports on the utilization of phosphine-ligand-stabilized, modified gold-coated magnetic nanoparticles as catalysts for the reduction and subsequent extraction of methylene blue in wastewater from the textile industry. These nanomaterials exhibit the ability to not only reduce the presence of toxic methylene blue dye in textile wastewater but also effectively eliminate the dye from the wastewater solution [23].

Gupta and Kulkarni have successfully prepared a porous foam of poly (dimethylsiloxane) (PDMS) embedded with Au nanoparticles for the purpose of eliminating organic compounds from water. The results showed that Au-PDMS nanocomposite foam was significantly effective against odorous sulfur-containing contaminants and was resistant to harsh chemical environments [24].

Methylene blue (MB) is a heterocyclic aromatic chemical that exists as a dark green powder. It is widely used in biology, chemistry, and the textile dyeing industry. It has been present in human and veterinary pharmacopeia for a long time. In the end, MB is discharged into the nearby environment causing real health problems. Exposure to MB can cause injuries to humans and animals [25]. It can also cause nausea, vomiting, and mental confusion. Direct contact can lead to eye burns, while inhalation leads to rapid or difficult breathing [26]. In this research, our objective is to incorporate Au⁰@PPh₂-PIILP into nanofibers of polyethylene terephthalate (PET) in order to create a nanogold composite (NGC) capable of efficiently eliminating methylene blue (MB) from wastewater. The whole process is illustrated in Scheme 1.



Scheme 1. Preparation of nanogold composite NGC adsorbent.

2. Materials and Methods

2.1. Preparation of $Au^0@PPh_2\text{-PIILP}$

$Au^0@PPh_2\text{-PIILP}$ was synthesized following established protocols and was fully characterized in previous studies (Figure 1) [27–29].

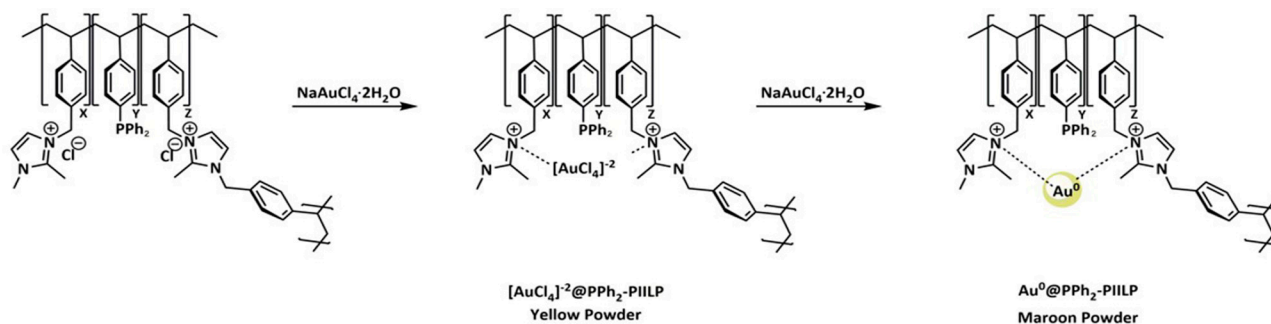


Figure 1. Reaction scheme for polymer-immobilized ionic liquids, and their $[AuCl_4]^{-}$ and nanogold-loaded counterparts.

2.2. Preparation of PET Nanofibers

PET nanofibers were produced by electrospinning using post-used PET cups as we described previously [30]. The electrospinning process was modified by adjusting several factors. The flow rate was established at 1 mL/h, the needle-to-collector distance was set at 15 cm, the PET concentration was maintained at 5%, and an applied voltage of 15 kV was utilized [31].

2.3. Preparation of Nanogold Composite NGC

Nanogold composite NGC was prepared by treating (0.03 g) of PET-NF with (1 mL, 0.5 M sodium hydroxide (NaOH, 98%) followed by 5 mL of distilled water. The purpose of NaOH treatment is to activate the fiber surface to be hydrophilic, allowing the coating of NF by $Au^0@PPh_2\text{-PIILP}$ in an aqueous solution [32]. The mixture was allowed to agitate at an ambient temperature for a duration of 30 min. Following the treatment process, the fibers were washed thoroughly with distilled water multiple times and subsequently air-dried at room temperature for a duration of 24 h. After drying, PET-NF was immersed in an aqueous solution of 0.003 g $Au^0@PPh_2\text{-PIILP}$ and 3 mL D.W Distilled water in a glass petri dish (\varnothing 18 cm) and left to dry at room temperature for 48 h.

2.4. Characterization of Nanogold Composite NGC

The functional groups present in the synthesized nano-adsorbents were analyzed using Fourier-transform infrared spectroscopy (FTIR). The analysis was carried out using a Shimadzu-IR Prestige-21 spectrophotometer (Columbia, MD, USA) with KBr powder pellets. Field Emission Scanning Electron Microscopy (FE-SEM) (Quanta 4500, Hillsboro, OR, USA) was utilized to investigate morphology and particle spreading. To determine morphology and size formation, transmission electron microscopy (TEM) was utilized using a Jeo 1/JEM 2100 electron microscope type Jeo 1/JEM 2100 (Akishima, Japan) was utilized. The synthesized nanostructures underwent chemical characterization through analysis by Energy Dispersive X-ray Spectroscopy (EDAX) and Elements Distribution Mapping (EDM).

2.5. MB Adsorption Batch Studies

Batch adsorption experiments were carried out to assess the capacity of NGC to adsorb methylene blue (MB) dye. The impact of different experimental factors was analyzed to determine the efficiency of NGC in eliminating MB dye.

2.5.1. pH Effect

To examine the impact of the initial pH of the solution on the adsorption of MB, 3 mL of a 10 mg L⁻¹ MB solution was introduced to 0.006 g of NGC at varying pH levels (4.0, 5.0, 6.0, and 8.0) while being stirred at a rate of 150 rpm for 1 h utilizing a DLAB magnetic stirrer model MS7-H550-pro. The solution was permitted to settle, and subsequently, the residual MB concentration in the supernatant solution was quantified using a JANEWAY 7315 Spectrophotometer (Vernon Hills, IL, USA) with a λ_{\max} of 660 nm. The concentrations of MB were calculated by comparing the resulting absorbance values with the MB standard calibration curve. Equations (1) and (2) were used to calculate the adsorption capacity of MB adsorbed onto NGC (q) at equilibrium and at a specific time, respectively. Equation (3) was used to calculate MB percent removal ($R\%$) [33]:

$$q_e = \frac{(C_i - C_e) * V}{M} \quad (1)$$

$$q_t = \frac{(C_i - C_t) * V}{M} \quad (2)$$

$$R\% = \frac{C_i - C_e}{C_i} \times 100 \quad (3)$$

The equilibrium and specific time adsorption capacities of MB are denoted as q_e and q_t , respectively. The initial and equilibrium concentrations of MB in the solution are represented by C_i and C_e (mg L⁻¹). V refers to the volume (L) of the experimental solution. M indicates the weight (g) of the NGC, while $R\%$ represents the removal percentage.

2.5.2. Initial Concentration Effect on MB Adsorption

The influence of initial concentration on the adsorption of MB onto NGC was investigated by combining 0.006 g of NGC with 3 mL of various initial MB concentrations (10, 20, 30, and 40 mg L⁻¹). The resulting mixture was subjected to stirring at a rate of 150 rpm for a duration of 1 h, maintaining a pH of 8 and room temperature conditions.

2.5.3. Adsorbent Dosage Effect on MB Adsorption

The influence of the amount of adsorbent used on the removal of MB was investigated by mixing different dosages of NGC (0.001, 0.002, 0.006, and 0.008 g) with 3 mL of 10 mg L⁻¹ MB at pH 8. The mixture was stirred for 1 h at a rate of 150 rpm under room temperature conditions.

2.6. Kinetic Studies

In this study, adsorption kinetic experiments were conducted under different time intervals ranging from 10 to 80 min. The pH was maintained at 8, while the amount of NGC used was 0.006 g, and the temperature remained constant throughout the experiments. The main objective of this investigation was to gain insights into the adsorption kinetics of MB on NGC by exploring four fundamental kinetic mechanisms. These mechanisms included the pseudo-first-order Equation (4), the pseudo-second-order Equation (5), the Elovich Equation (6), and the intraparticle diffusion Equation (7). By examining these mechanisms, a comprehensive understanding of the adsorption kinetics of MB on NGC could be achieved [34–36].

$$\log(q_e - q_t) = \log q_e - \left(\frac{k_1}{2.303} \right) t \quad (4)$$

$$\frac{t}{q_t} = \frac{1}{k_2 q_e^2} + \frac{1}{q_e} (t) \quad (5)$$

$$q_t = \frac{1}{\beta} \ln(\alpha\beta) + \frac{1}{\beta} \ln(t) \quad (6)$$

$$q_t = K_{dif} t^{\frac{1}{2}} + B_L \quad (7)$$

In the time frame denoted as t , the rate constants for the pseudo-first-order and pseudo-second-order models are denoted as k_1 (min^{-1}) and k_2 ($\text{g mg}^{-1} \text{min}^{-1}$), respectively. Furthermore, α represents the initial adsorption rate (mg g^{-1}), while β represents the desorption constant (g mg^{-1}). Additionally, K_{dif} signifies the intraparticle diffusion rate constant ($\text{mg g}^{-1} \text{min}^{-1/2}$), and B_L refers to the boundary layer thickness.

2.7. Effect of Different Concentrations and Temperatures

The study examined the impact of different concentrations (10, 20, 30, and 40 mg L^{-1}) and temperatures (20, 30, 40, and 50 $^{\circ}\text{C}$) on batch MB adsorption experiments on NGC at pH 8. To effectively analyze the adsorption isotherms, four distinct models were employed: Langmuir Equation (8), Freundlich Equation (9), Temkin Equation (10), and Dubinin–Radushkevich Equation (11). Understanding patterns in adsorption isotherms is essential for optimizing adsorption systems and improving mechanisms of the adsorption process [35,37].

$$\frac{1}{q_e} = \left(\frac{1}{k_L Q_m} \right) \frac{1}{C_e} + \frac{1}{Q_m} \quad (8)$$

$$\log q_e = \log K_f + \frac{1}{n} \log C_e \quad (9)$$

$$q_e = B_T \ln A_T + B_T \ln C_e \quad (10)$$

$$\ln q_e = \ln Q_m - K_{D-R} \quad (11)$$

where Q_m refers to the maximum monolayer capacity (mg g^{-1}), while K_L (L mg^{-1}), K_f (L g^{-1}), A_T (L mg^{-1}), and K_{D-R} represent the equilibrium rate constants for Langmuir, Freundlich, Temkin, and Dubinin–Radushkevich, respectively. The parameter $1/n$ represents the intensity of the adsorption process.

3. Results and Discussion

3.1. Characterization of Nanogold Composite NGC

3.1.1. Fourier-Transform Infrared Spectroscopy (FTIR)

The FTIR spectrum of NGC before MB adsorption shows that five bands are observed, as in Figure 2, which reveal stacked spectra of NGC after adsorption (black) and before adsorption (red). The characteristic bands highlight alterations in band intensities rather than any noticeable shifts. For instance, the 3400 cm^{-1} bands denote ν (O–H) stretching, the 2921 cm^{-1} bands denote ν (C–H) stretching, and the band at 1700 cm^{-1} can be assigned to (C–N) stretching. The band at 1261 cm^{-1} indicates ν (C=O) stretching, while 1095 cm^{-1} indicates ν (C=C aromatic) stretching. Notably, the band related to (C=O) stretching displays a downward shift at 1243 cm^{-1} of approximately 20 cm^{-1} in frequency after adsorption. This suggests a significant hydrogen-bonding interaction between C=O and MB [38]. The vibrational modes of the (C=C aromatic) stretching band before adsorption shifted to 1044 cm^{-1} implying modification of ring vibration, which is indicative of interactions like pi–pi interactions with MB [39].

As the composite structure comprises polymers, the movement of these polymer frameworks could potentially immobilize the nanogold. This dual functionality is anticipated to hinder the aggregation of nanoparticles and fibers and contribute to maintaining small particle size and stability [40].

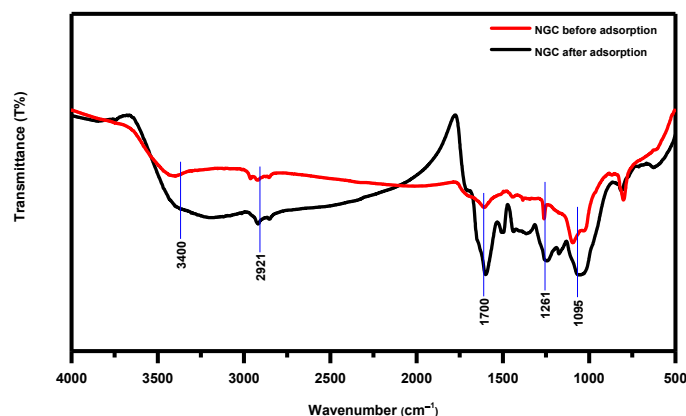


Figure 2. FTIR spectra obtained both before and after adsorption of MB by NGC.

3.1.2. Field Emission Scanning Electron Microscopy (FE-SEM)

The surface morphologies of Au⁰@PPh₂-PIILP, PET-NF, and NGC were characterized by FE-SEM (Figure 3a–c). Figure 3a revealed a smooth surface architecture and this assured the successful preparation of Au⁰@PPh₂-PIILP [28]. Figure 3b shows that the diameter of a PET-NF electrospun nanofiber is less than 100 nm [41]. Figure 3c suggests that self-assemblies are formed between PET-NF and Au⁰@PPh₂-PIILP. Also, the micrographs demonstrate PET-NF coated by Au⁰@PPh₂-PIILP molecules over the PET-NF surface under reaction conditions.

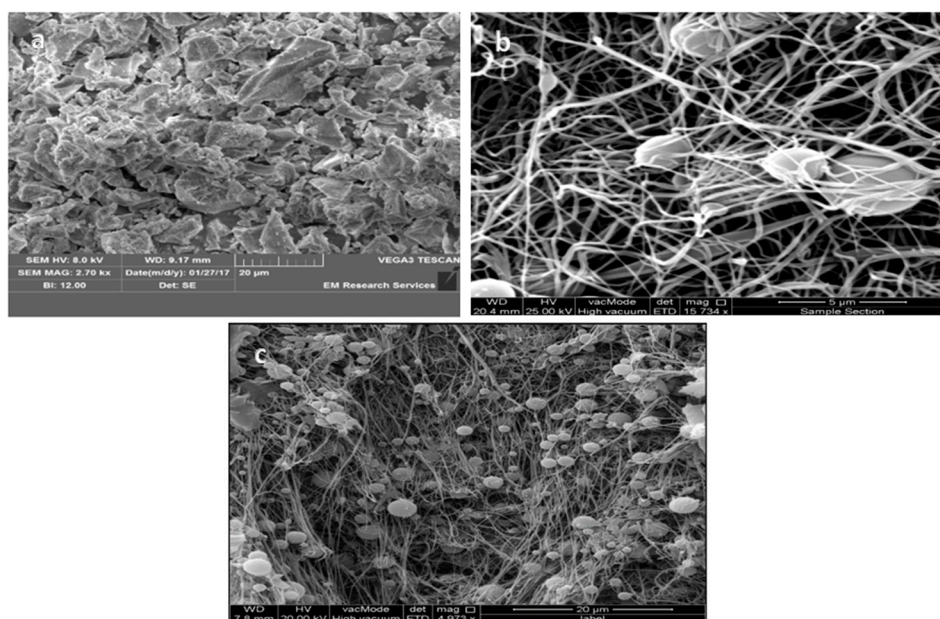


Figure 3. FE-SEM of (a) Au⁰@PPh₂-PIILP; (b) PET-NF; and (c) NGC.

3.1.3. Transmission Electron Microscopy (TEM)

The utilization of TEM measurement provides advantages in visualizing the morphology and structure of individual nanocomposites resulting from the combination of Au⁰@PPh₂-PIILP and PET-NF. Figure 4 serves as evidence confirming the successful formation of the composite. NGC composites exhibit distinct morphologies and decrease in particle size for each specimen due to an increased quantity of gold particles (Figure 4a); this characteristic may also be linked to the polyphenolic composition of PPh₂-PIILP [42]. A higher quantity of MB absorbed onto NGC reveals heterogeneous, uneven particles of varying sizes and shapes. (Figure 4b).

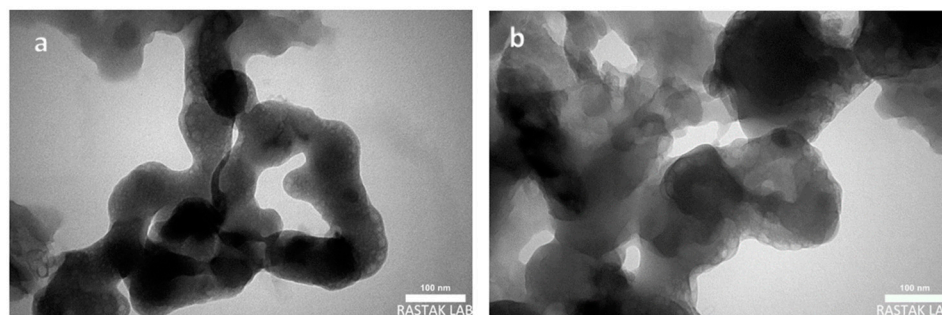


Figure 4. TEM images of NGC (a) before adsorption and (b) after adsorption.

3.1.4. Energy Dispersive X-ray Spectroscopy (EDAX) and Elements Distribution Mapping (EDM)

Chemical composition analysis of NGC was carried out using Energy Dispersive X-ray Spectroscopy (EDAX) and Elements Distribution Mapping (EDM). The EDAX spectra of NGC (Figure 5a) displayed elemental peaks corresponding to oxygen, carbon, and gold, with weight compositions of 47.268%, 21.076%, and 31.654%, respectively, confirming the composite nature of the material. Subsequent analysis of atomic compositions unveiled that oxygen, carbon, and gold accounted for 49.839%, 26.106%, and 24.053% of the total composition, respectively. The images obtained through EDAX and EDM indicated a uniform distribution of gold within the composite material (Figure 5b,c) [43].

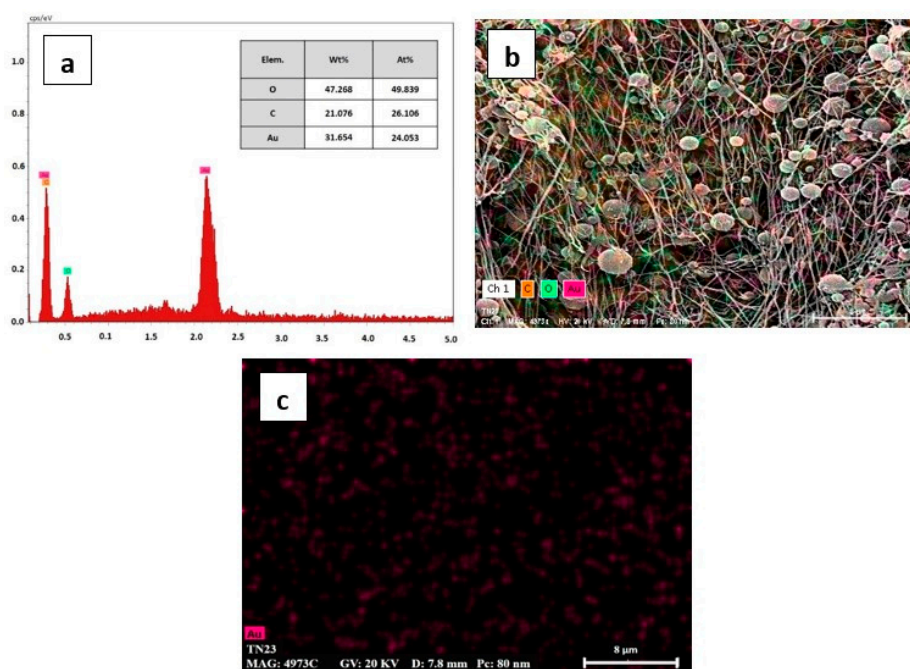


Figure 5. (a,b) EDAX spectrum of NGC; (c) map of gold distribution in NGC.

3.2. Batch Studies

3.2.1. Effect of pH on Adsorption

Figure 6 demonstrates a comparison of NGC's capacity to absorb MB at different pH levels. The removal efficiency $R\%$ of MB increased from 3.134% to 83.647% as the pH level rose from 4 to 8, with the highest adsorption of MB (83.647%) achieved at pH 8. The increase in pH resulted in the deprotonation of the composite material, leading to a negative charge. This change in charge enhanced the material's electrostatic attraction affinity towards the cationic MB dye, consequently, increasing the adsorption capacity. Conversely, at low pH levels, protonation of the composite material created a competitor to the cationic MB dye, reducing adsorption capacity. These observations can be explained by

the protonation and deprotonation processes of the composite material, which align with previous studies [44–46].

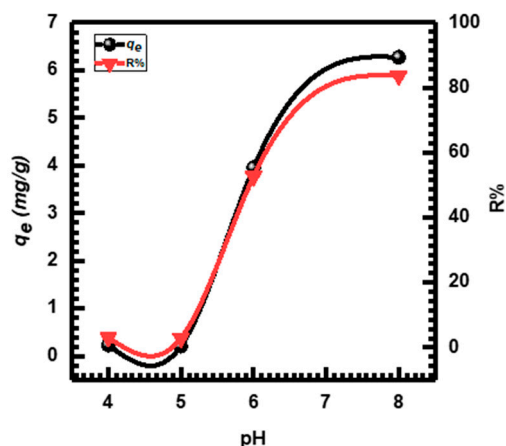


Figure 6. The impact of pH on MB adsorption onto NGC.

3.2.2. Effect of Concentration on MB Adsorption

The impact of the initial concentration of MB, ranging from 10 to 40 mg L⁻¹, on the process of adsorption was investigated. Figure 7 displays the relationship between MB adsorption and adsorbent concentration. It is clear that as the concentration of the adsorbent increases, the amount of MB adsorbed also increases. However, the percentage of MB removal decreases with higher initial concentrations of MB. An increase in the initial concentration of MB promotes a stronger interaction between MB and NGC, resulting in a higher uptake of adsorption. These findings are consistent with previous studies [47,48].

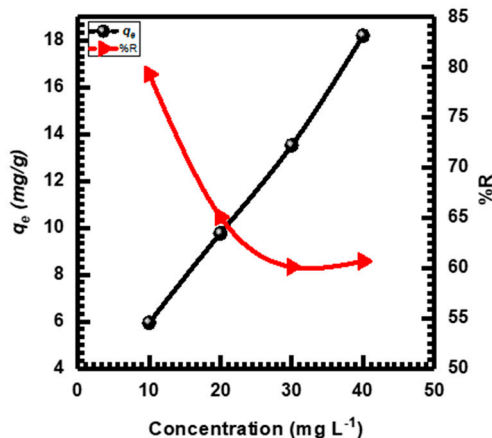


Figure 7. The impact of concentration on the adsorption of MB on NGC.

3.2.3. Effect of Dosage on MB Adsorption

The information presented in Figure 8 demonstrates changes in q_e values with varying doses of NGC. It was noted that as the NGC dose increased, the adsorption capacity q_e decreased. Specifically, the decrease in q_e from 25.709 to 3.207 mg g⁻¹ was observed as the adsorbate dose rose from 0.001 to 0.008 g. This decline can be explained by the competition among adsorbates for adsorption and the distribution of the concentration gradient between the solute in solution and the solute at the adsorbate's surface. Moreover, the covering of adsorption sites due to a decrease in available surface area for adsorption and an increase in the diffusion pathway also played a role in this reduction. Consequently, the quantity of MB adsorbed per unit weight of NGC decreased, leading to a decrease in adsorption capacity [49,50].

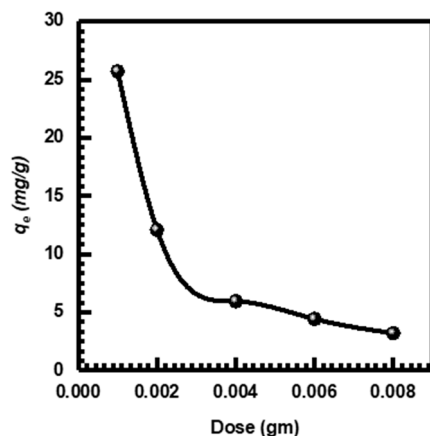


Figure 8. The impact of varying dosages on the adsorption of MB onto NGC.

3.2.4. Effect of Contact Time on MB Adsorption

The study examined the adsorption of MB dye at varying contact times (10–80 min) and discovered that the uptake of dye increased as contact time increased. Equilibrium was reached after 15 min (as shown in Figure 9). Based on these discoveries, the adsorption process initiates swiftly on the outer surface of the adsorbent, succeeded by a more gradual internal diffusion process, which ultimately governs the adsorption rate. Initially, adsorption occurs quickly due to the availability of numerous surface sites. However, as time progresses, accessibility of the remaining surface sites diminishes, causing the solute molecules in the solid and bulk phases to repel each other. Consequently, it takes a longer period to achieve equilibrium [51].

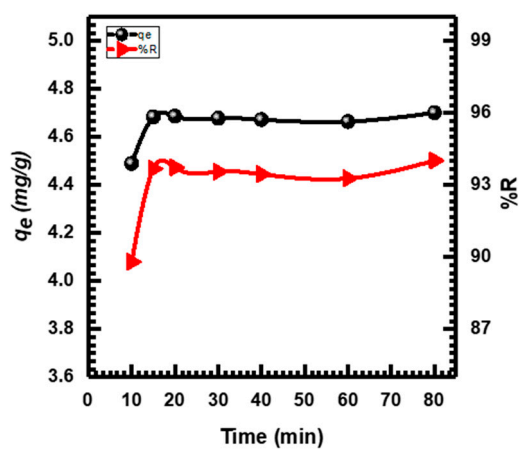


Figure 9. The impact of contact duration on the adsorption of MB onto NGC.

3.3. Kinetic Study of Adsorption

The progression of time reveals the nature of adsorption capability through adsorption kinetics. It is of utmost importance to determine the specific type of adsorption mechanism within a given system [52]. Table 1 provides a summary of the kinetic studies conducted on the adsorption of MB by NGC. Figure 10a illustrates kinetic plots for the pseudo-first-order adsorption of MB on NGC at constant temperatures and initial MB concentrations. The correlation coefficient R^2 value, which is 0.8951 as presented in Table 1, indicates a moderate fit. However, the calculated equilibrium sorption capacity q_e of 1.4949 does not align with the experimental data of 4.6838, as shown in Table 1. This discrepancy suggests that a pseudo-first-order model is not suitable for accurately predicting MB adsorption kinetics on NGC [53,54]. On the other hand, Figure 10b displays kinetic plots for the pseudo-second-order sorption kinetics of MB onto NGC. The calculated R^2 value of 0.9996 indicates an excellent fit, and the computed value of the equilibrium adsorption capacity, q_e , aligns well

with the experimental data. Therefore, the results strongly suggest that the adsorption of MB onto NGC follows a pseudo-second-order equation [55].

Table 1. The kinetic parameters related to the adsorption of MB onto NGC.

| K_1 | Pseudo-First-Order | | | K_2 | Pseudo-Second-Order | | | α | Elovich | | Intraparticle Diffusion | | |
|--------|--------------------|-----------------|--------|--------|---------------------|-----------------|--------|------------------------|---------|--------|-------------------------|-----------|--------|
| | $(q_e)_{exp.}$ | $(q_e)_{calc.}$ | R^2 | | $(q_e)_{exp.}$ | $(q_e)_{calc.}$ | R^2 | | β | R^2 | B_L | K_{dif} | R^2 |
| 0.0078 | 4.6838 | 1.4949 | 0.8951 | 0.1893 | 4.6838 | 4.3840 | 0.9996 | 1.964×10^{12} | 8.0775 | 0.9525 | 3.7679 | 0.0752 | 0.8912 |

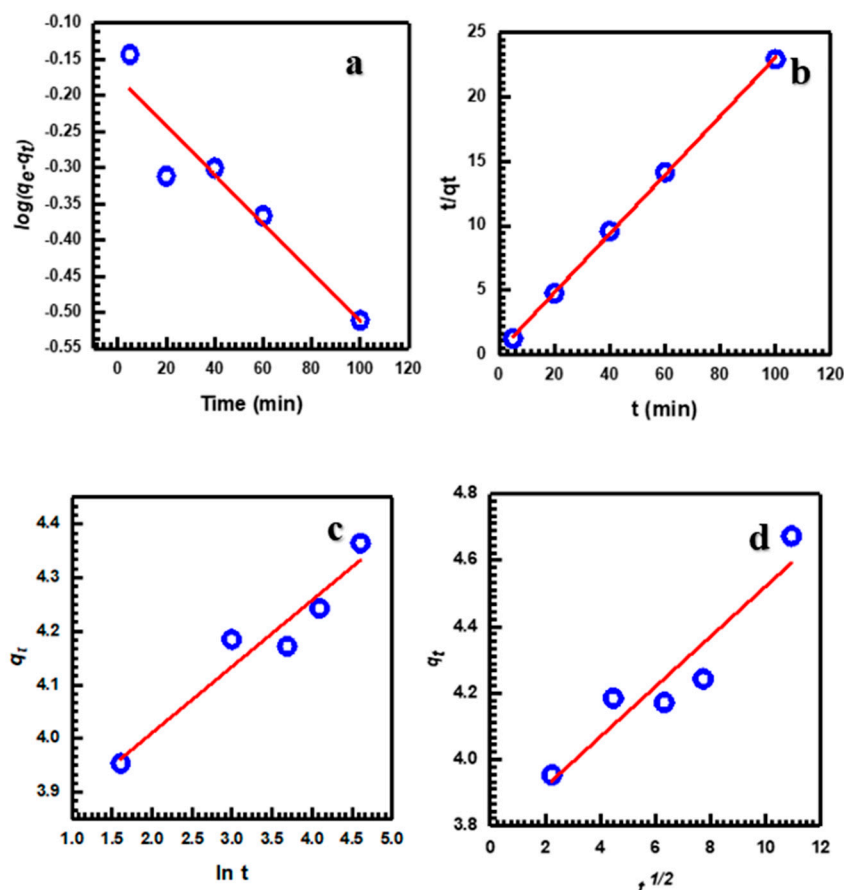


Figure 10. Pseudo-first-order (a), pseudo-second-order (b), Elovich (c), and intraparticle diffusion (d) kinetics of the adsorption of MB on NGC.

The Elovich Equation, which is commonly used to describe adsorption capacity, is presented in Table 1. A graphical representation in Figure 10c showcases the relationship between q_t and $\ln(t)$. The Elovich constants, α and β , were determined by analyzing the intercept and slope, respectively, and their values are documented in Table 1. The correlation coefficient value of 0.9252 indicates the suitability of the Elovich model [56]. Figure 10d illustrates the kinetics of MB intraparticle diffusion. From the plot of q_t against $t^{1/2}$, the values of K_{dif} and R^2 were determined as 0.0752 and 0.8912, respectively. The linearity observed in the plots (Figure 10d) suggests that intraparticle diffusion significantly contributes to the uptake of MB by NGC. This further confirms that the adsorption of MB onto NGC involves a multi-step process within its interior [57].

Furthermore, this interdependent relationship also suggests that the adsorption of MB on NGC occurred through a complex series of steps. When these steps are clearly distinguishable, the graph typically exhibits multiple intersecting lines. The initial line represents adsorption on the surface, while the subsequent lines illustrate intraparticle diffusion. Conversely, the absence of such distinct features in the graph indicates that the steps are not easily discernible, implying that intraparticle diffusion has been the predominant process right from the beginning of the interaction between MB and NGC.

However, this information alone does not provide sufficient details to determine which of these two phases serves as the rate-limiting step [58]. Additionally, the intercept B_L value reveals that as the thickness of the boundary layer increases, the impact of the boundary layer becomes more pronounced. In simpler terms, when the intercept B_L value in the data rises, the amount of solute adsorbed on the boundary layer also increases. Table 1 presents the B_L value, which is obtained by calculating the intercept of linear plots of q_t versus $t^{1/2}$ under all experimental conditions [59].

3.4. Isotherm Study of Adsorption

Evaluation of the transfer of dye molecules from a solution to adsorbent particles at equilibrium is commonly conducted through an analysis of adsorption isotherms. Among various approaches, adsorption isotherm analysis is widely recognized as the most efficient and valuable method. In Figure 11, the adsorption of MB on NGC is visually depicted, while the parameters for each isotherm are presented in Table 2. These parameters are derived from the slopes and intercepts of the plots. To determine the most appropriate isotherm for the experimental data, the isotherm exhibiting the highest correlation coefficient (R^2) was selected, indicating its strong correlation with the data [60].

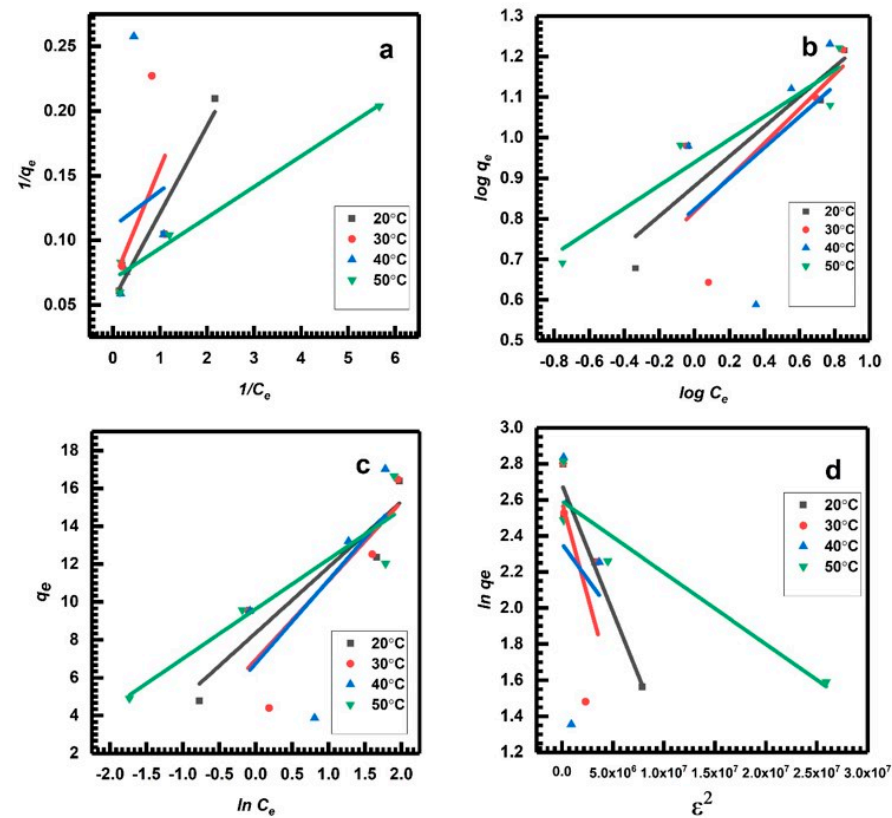


Figure 11. Illustrations of the Langmuir isotherm (a), Freundlich isotherm (b), Tempkin isotherm (c), and Dubinin-Radosevich (d) isotherm of the adsorption of MB on NGC.

Table 2. The isotherm parameters for the adsorption of MB onto NGC.

| Temp. °C | Langmuir Parameters | | | Freundlich Parameters | | | Tempkin Parameters | | | | Dubinin–Radosevich | | |
|----------|---------------------|--------|-------|-----------------------|-------|-------|--------------------|-------|----------|-------|--------------------|--------------------|-------|
| | K_L | Q_m | R^2 | K_f | n | R^2 | A_T | B_T | b_T | R^2 | Q_m | K_{D-R} | R^2 |
| 20 | 0.797 | 18.622 | 0.938 | 7.596 | 2.969 | 0.860 | 11.098 | 3.474 | 724.953 | 0.895 | 14.656 | 1×10^{-7} | 0.955 |
| 30 | 0.766 | 14.771 | 0.314 | 1.913 | 2.365 | 0.573 | 4.655 | 4.517 | 576.045 | 0.698 | 13.305 | 2×10^{-7} | 0.373 |
| 40 | 4.025 | 9.033 | 0.015 | 6.663 | 2.625 | 0.217 | 4.661 | 4.393 | 611.281 | 0.384 | 10.562 | 8×10^{-8} | 0.037 |
| 50 | 1.338 | 14.265 | 0.975 | 6.221 | 7.793 | 0.907 | 106.817 | 2.062 | 1100.561 | 0.867 | 13.356 | 4×10^{-8} | 0.893 |

The results obtained indicated that the Langmuir model was followed by the adsorption of MB due to the strong coefficient correlation (R^2). Consequently, a monolayer of MB is expected to be formed on the surface of the NGC as the potential adsorption mechanism. Additionally, the (R^2) values also demonstrated that MB adsorption on NGC did not adhere to the Freundlich, Temkin, or Dubinin–Radosevich isotherms, as shown in Table 2. Generally, if $n > 1$, it suggests that the adsorbate is favorably adsorbed on the adsorbent. The fact that in our study n is significantly greater than unity at all investigated temperatures indicates that NGC is a suitable adsorbent for the adsorption of MB from an aqueous solution [61].

The Temkin model is not suitable for representing the equilibrium isotherms of MB on NGC due to the low R^2 values. In contrast, the Dubinin–Radushkevich (D–R) model was employed to determine the apparent free energy of adsorption (E), which is commonly used to differentiate between physical and chemical adsorption. The adsorption energy calculated from the D–R isotherms for MB on NGC indicated physical adsorption [62–64], with Q_m values decreasing as temperature increased, suggesting an exothermic adsorption process [65].

Table 3 presents a comparison of the adsorption capacities Q_m achieved in this investigation with various types of MB adsorbents in previous research studies.

Table 3. A comparative analysis of the adsorption capacities Q_m for various types of adsorbents used in previous studies to remove MB.

| Adsorbent Material | Q_m | Time | pH | [Ref.] |
|---|--------|---------|-----|------------|
| Cellulose nanostructure | 4.369 | 120 min | 6.0 | [49] |
| PET-NF/MWCNTs | 7.047 | 120 min | 8.0 | [19] |
| Modified PET-NF | 13.774 | 100 min | 6.0 | [37] |
| Nanogold composite NGC | 18.622 | 80 min | 8.0 | This study |
| CuO NPs | 26.73 | 120 min | 8.0 | [15] |
| Fe ₃ O ₄ @MIL-100(Fe) | 49 | 400 min | 2.0 | [66] |
| Nanoparticles of microalgae | 58.820 | 180 min | 6.0 | [67] |

The adsorption of dyes involves various mechanisms such as ion exchange, hydrogen bonding, Van der Waals forces, electrostatics, and dipole–ion interactions. The results from the kinetic and isotherm studies suggest that physical attraction is the main adsorption mechanism for MB onto NGC. Therefore, it can be inferred that the primary mechanism of adsorption is electrostatic interactions [68].

4. Conclusions

A novel approach was employed to synthesize a nanogold composite (NGC) by combining polyethylene terephthalate (PET) nanofibers with Au⁰@PPh₂-PIILP. This groundbreaking research marks the first successful integration of these materials, resulting in a highly efficient NGC for the removal of methylene blue (MB) from wastewater.

Through the study, the optimal conditions for MB dye removal were determined to be a pH of eight, an adsorbent dosage of 0.006 g, an initial MB concentration of 10 mg L⁻¹, and a treatment time of 80 min. The adsorption process followed a pseudo-second-order kinetic model, providing a comprehensive description. Additionally, there was a strong agreement between the calculated adsorption capacity ($(q_e)_{cal}$. (4.3840) and the experimental adsorption capacity ($(q_e)_{exp}$. (4.6838). The Langmuir isotherm also demonstrated a good fit to the data, indicating a maximum adsorption capacity of 18.622 mg g⁻¹ for MB. The sole constraint in this study lies in the utilization of gold and its costly nature. Therefore, we urge researchers to explore alternative elements that offer comparable effectiveness at a more affordable cost for the elimination of methylene blue.

Author Contributions: Conceptualization, S.A.Y. and E.A.A.; methodology, S.A.Y. and W.K.E.; software, A.A.; validation, E.A.A., S.A.Y. and W.K.E.; formal analysis, S.A.Y. and E.A.A.; investigation, W.K.E. and A.A.; resources, A.A.; data curation, W.K.E. and A.A.; writing—original draft preparation, W.K.E. and S.A.Y.; writing—review and editing, W.K.E. and A.A.; visualization, S.A.Y. and E.A.A.; supervision, S.A.Y. All authors have read and agreed to the published version of the manuscript.

Funding: The authors are thankful for the financial support provided by the USAID Partnerships for Enhanced Engagement in Research (PEER) Program (PEER/Iraq project/cycle 6).

Institutional Review Board Statement: Not applicable.

Informed Consent Statement: Not applicable.

Data Availability Statement: The data presented in this study are available in the article.

Acknowledgments: The authors are thankful for the USAID Partnerships for Enhanced Engagement in Research (PEER) laboratory for supporting this work at the University of Duhok.

Conflicts of Interest: The authors declare no conflicts of interest.

References

1. Bashir, I.; Lone, F.A.; Bhat, R.A.; Mir, S.A.; Dar, Z.A.; Dar, S.A. Concerns and Threats of Contamination on Aquatic Ecosystems. In *Bioremediation and Biotechnology: Sustainable Approaches to Pollution Degradation*; Hakeem, K.R., Bhat, R.A., Qadri, H., Eds.; Springer International Publishing: Cham, Switzerland, 2020; pp. 1–26. [\[CrossRef\]](#)
2. Mishra, R.K. Fresh water availability and its global challenge. *Br. J. Multidiscip. Adv. Stud.* **2023**, *4*, 1–78. [\[CrossRef\]](#)
3. Khraisheh, M.; Elhenawy, S.; AlMomeni, F.; Al-Ghouti, M.; Hassan, M.K.; Hameed, B.H. Recent Progress on Nanomaterial-Based Membranes for Water Treatment. *Membranes* **2021**, *11*, 995. [\[CrossRef\]](#) [\[PubMed\]](#)
4. Azzaz, A.A.; Jellali, S.; Hamed, N.B.H.; El Jery, A.; Khezami, L.; Assadi, A.A.; Amrane, A. Photocatalytic Treatment of Wastewater Containing Simultaneous Organic and Inorganic Pollution: Competition and Operating Parameters Effects. *Catalysts* **2021**, *11*, 855. [\[CrossRef\]](#)
5. Tang, M.; Xu, R.; Gong, Y.; Zhang, H.; He, J.; Wu, P.; Liu, C.; Jiang, W. Treatment of Variable Complex Mixed Dye Wastewater by Photodegradation with a Photocatalyst Gradation Strategy. *Ind. Eng. Chem. Res.* **2021**, *60*, 17520–17533. [\[CrossRef\]](#)
6. Sukmana, H.; Bellahsen, N.; Pantoja, F.; Hodur, C. Adsorption and coagulation in wastewater treatment—Review. *Prog. Agric. Eng. Sci.* **2021**, *17*, 49–68. [\[CrossRef\]](#)
7. Sales, F.R.P.; Serra, R.B.G.; de Figueirêdo, G.J.A.; da Hora, P.H.A.; de Sousa, A.C. Wastewater treatment using adsorption process in column for agricultural purposes. *Rev. Ambiente Água* **2019**, *14*, 1–9. [\[CrossRef\]](#)
8. Nawaz, M.S.; Son, H.S.; Jin, Y.; Kim, Y.; Soukane, S.; Al-Hajji, M.A.; Abu-Ghdaib, M.; Ghaffour, N. Investigation of flux stability and fouling mechanism during simultaneous treatment of different produced water streams using forward osmosis and membrane distillation. *Water Res.* **2021**, *198*, 117157. [\[CrossRef\]](#)
9. Farid, M.U.; Kharraz, J.A.; Sun, J.; Boey, M.; Riaz, M.A.; Wong, P.W.; Jia, M.; Zhang, X.; Deka, B.J.; Khanzada, N.K. Advancements in nanoenabled membrane distillation for a sustainable water-energy-environment nexus. *Adv. Mater.* **2024**, *36*, 2307950. [\[CrossRef\]](#) [\[PubMed\]](#)
10. Chen, L.; Xue, Y.; Luo, T.; Wu, F.; Alshwabkeh, A.N. Electrolysis-assisted UV/sulfite oxidation for water treatment with automatic adjustments of solution pH and dissolved oxygen. *Chem. Eng. J.* **2021**, *403*, 126278. [\[CrossRef\]](#)
11. Lourinho, G.; Brito, P.S.D. Electrolytic treatment of swine wastewater: Recent progress and challenges. *Waste Biomass Valorization* **2021**, *12*, 553–576. [\[CrossRef\]](#)
12. Obotey Ezugbe, E.; Rathilal, S. Membrane technologies in wastewater treatment: A review. *Membranes* **2020**, *10*, 89. [\[CrossRef\]](#) [\[PubMed\]](#)
13. Lech, M.; Klimek, A.; Porzybót, D.; Trusek, A. Three-Stage Membrane Treatment of Wastewater from Biodiesel Production—Preliminary Research. *Membranes* **2021**, *12*, 39. [\[CrossRef\]](#) [\[PubMed\]](#)
14. Agarwala, R.; Mulky, L. Adsorption of dyes from wastewater: A comprehensive review. *ChemBioEng Rev.* **2023**, *10*, 326–335. [\[CrossRef\]](#)
15. Essa, W.K. Methylene Blue Removal by Copper Oxide Nanoparticles Obtained from Green Synthesis of *Melia azedarach*: Kinetic and Isotherm Studies. *Chemistry* **2024**, *6*, 249–263. [\[CrossRef\]](#)
16. Irshad, M.A.; Nawaz, R.; Wojciechowska, E.; Mohsin, M.; Nawrot, N.; Nasim, I.; Hussain, F. Application of nanomaterials for cadmium adsorption for sustainable treatment of wastewater: A review. *Water Air Soil Pollut.* **2023**, *234*, 54. [\[CrossRef\]](#)
17. Elsaid, K.; Olabi, A.G.; Abdel-Wahab, A.; Elkamel, A.; Alami, A.H.; Inayat, A.; Chae, K.-J.; Abdelkareem, M.A. Membrane processes for environmental remediation of nanomaterials: Potentials and challenges. *Sci. Total Environ.* **2023**, *879*, 162569. [\[CrossRef\]](#) [\[PubMed\]](#)
18. Khatri, M.; Francis, L.; Hilal, N. Modified electrospun membranes using different nanomaterials for membrane distillation. *Membranes* **2023**, *13*, 338. [\[CrossRef\]](#) [\[PubMed\]](#)

19. Essa, W.K.; Yasin, S.A.; Abdullah, A.H.; Thalji, M.R.; Saeed, I.A.; Assiri, M.A.; Chong, K.F.; Ali, G.A.M. Taguchi L25 (5⁴) Approach for Methylene Blue Removal by Polyethylene Terephthalate Nanofiber-Multi-Walled Carbon Nanotube Composite. *Water* **2022**, *14*, 1242. [[CrossRef](#)]
20. Lim, C.T. Nanofiber technology: Current status and emerging developments. *Prog. Polym. Sci.* **2017**, *70*, 1–17. [[CrossRef](#)]
21. Sharma, G.K.; Joseph, S.L.; MS, A.; James, N.R. Tellurium Nanoparticles Incorporated into Electrospun Poly (acrylonitrile) Nanofibers, Followed by Carbonization and Their Poly (dimethylsiloxane) Composites for Electromagnetic Interference Shielding. *ACS Appl. Nano Mater.* **2024**, *7*, 5819–5830. [[CrossRef](#)]
22. Beyene, H.D.; Ambaye, T.G. Application of Sustainable Nanocomposites for Water Purification Process BT. In *Sustainable Polymer Composites and Nanocomposites*; Inamuddin, Thomas, S., Mishra, R.K., Asiri, A.M., Eds.; Springer International Publishing: Cham, Switzerland, 2019; pp. 387–412. [[CrossRef](#)]
23. Lukhele, E.J.; Khutlane, J.T.; Báthori, N.B.; Malgas-Enus, R. Reduction and removal of methylene blue from aqueous solutions via recyclable magnetic gold nanomaterials. *Surf. Interfaces* **2022**, *31*, 101970. [[CrossRef](#)]
24. Gupta, R.; Kulkarni, G.U. Removal of organic compounds from water by using a gold nanoparticle–poly (dimethylsiloxane) nanocomposite foam. *ChemSusChem* **2011**, *4*, 737–743. [[CrossRef](#)] [[PubMed](#)]
25. Wibowo, Y.G.; Syahnur, M.T.; Al-Azizah, P.S.; Gintha, D.A.; Lululangi, B.R.G. Phytoremediation of high concentration of ionic dyes using aquatic plant (*Lemna minor*): A potential eco-friendly solution for wastewater treatment, Environmental Nanotechnology. *Monit. Manag.* **2023**, *20*, 100849. [[CrossRef](#)]
26. Besharati, N.; Alizadeh, N.; Shariati, S. Removal of cationic dye methylene blue (MB) from aqueous solution by Coffee and Peanut husk Modified with Magnetite Iron Oxide Nanoparticles. *J. Mex. Chem. Soc.* **2018**, *62*, 110–124. [[CrossRef](#)]
27. Doherty, S.; Knight, J.G.; Backhouse, T.; Abood, E.; Alshaikh, H.; Fairlamb, I.J.S.; Bourne, R.A.; Chamberlain, T.W.; Stones, R. Highly efficient aqueous phase chemoselective hydrogenation of α , β -unsaturated aldehydes catalysed by phosphine-decorated polymer immobilized IL-stabilized PdNPs. *Green Chem.* **2017**, *19*, 1635–1641. [[CrossRef](#)]
28. Doherty, S.; Knight, J.G.; Backhouse, T.; Abood, E.; Al-shaikh, H.; Clemmet, A.R.; Ellison, J.R.; Bourne, R.A.; Chamberlain, T.W.; Stones, R. Heteroatom Donor-Decorated Polymer-Immobilized Ionic Liquid Stabilized Palladium Nanoparticles: Efficient Catalysts for Room-Temperature Suzuki-Miyaura Cross-Coupling in Aqueous Media. *Adv. Synth. Catal.* **2018**, *360*, 3716–3731. [[CrossRef](#)]
29. Doherty, S.; Knight, J.G.; Backhouse, T.; Summers, R.J.; Abood, E.; Simpson, W.; Paget, W.; Bourne, R.A.; Chamberlain, T.W.; Stones, R. Highly selective and solvent-dependent reduction of nitrobenzene to N-phenylhydroxylamine, azoxybenzene, and aniline catalyzed by phosphino-modified polymer immobilized ionic liquid-stabilized AuNPs. *ACS Catal.* **2019**, *9*, 4777–4791. [[CrossRef](#)]
30. Abbas, J.A.; Said, I.A.; Mohamed, M.A.; Yasin, S.A.; Ali, Z.A.; Ahmed, I.H. Electrospinning of polyethylene terephthalate (PET) nanofibers: Optimization study using taguchi design of experiment. *IOP Conf. Ser. Mater. Sci. Eng.* **2018**, *454*, 012130. [[CrossRef](#)]
31. Yasin, S.A.; Zeebaree, S.Y.S.; Zeebaree, A.Y.S.; Zebari, O.I.H.; Saeed, I.A. The efficient removal of methylene blue dye using CuO/PET nanocomposite in aqueous solutions. *Catalysts* **2021**, *11*, 241. [[CrossRef](#)]
32. Patel, K.D.; Kim, T.-H.; Mandakhbayar, N.; Singh, R.K.; Jang, J.-H.; Lee, J.-H.; Kim, H.-W. Coating biopolymer nanofibers with carbon nanotubes accelerates tissue healing and bone regeneration through orchestrated cell-and tissue-regulatory responses. *Acta Biomater.* **2020**, *108*, 97–110. [[CrossRef](#)]
33. Yasin, S.; Ahmed, H.; Saleem, P.; Saeed, I. A Kinetic Study of Removing Methylene Blue from Aqueous Solutions by Modified Electrospun Polyethelene Terephthalate Nanofibres. *Egypt. J. Chem.* **2021**, *64*, 8–9. [[CrossRef](#)]
34. Adeyi, A.A.; Jamil, S.N.A.M.; Abdullah, L.C.; Choong, T.S.Y.; Lau, K.L.; Abdullah, M. Adsorptive removal of methylene blue from aquatic environments using thiourea-modified poly (acrylonitrile-co-acrylic acid). *Materials* **2019**, *12*, 1734. [[CrossRef](#)] [[PubMed](#)]
35. Najim, T.S.; Yasin, S.A.A.R. Adsorption of Cr (VI) from aqueous solution using low cost adsorbent: Equilibrium study. *Sci. J. Univ. Zakho* **2013**, *1*, 758–767.
36. Mosoarca, G.; Popa, S.; Vancea, C.; Boran, S. Optimization, equilibrium and kinetic modeling of methylene blue removal from aqueous solutions using dry bean pods husks powder. *Materials* **2021**, *14*, 5673. [[CrossRef](#)] [[PubMed](#)]
37. Ahmed, H.A.; Saleem, P.H.; Yasin, S.A.; Saeed, I.A. The application of modified polyethelene terphthalate (pet) nanofibers; characterization and isotherm study. *J. Phys. Conf. Ser.* **2021**, *1853*, 12006. [[CrossRef](#)]
38. Fu, J.; Chen, Z.; Wang, M.; Liu, S.; Zhang, J.; Zhang, J.; Han, R.; Xu, Q. Adsorption of methylene blue by a high-efficiency adsorbent (polydopamine microspheres): Kinetics, isotherm, thermodynamics and mechanism analysis. *Chem. Eng. J.* **2015**, *259*, 53–61. [[CrossRef](#)]
39. Liu, S.; Wang, C.; Song, Y.; Yan, B.; Ai, B.; Pan, K.; Zhang, L. Fabrication of a hybrid phase TiO₂/g-C₃N₄ heterojunction composite with enhanced adsorption and photocatalytic degradation of MB under visible light. *New J. Chem.* **2023**, *47*, 8170–8181. [[CrossRef](#)]
40. Bhatt, N.; Mehata, M.S. A Sustainable Approach to Develop Gold Nanoparticles with Kalanchoe Fedtschenkoi and Their Interaction with Protein and Dye: Sensing and Catalytic Probe. *Plasmonics* **2023**, *18*, 845–858. [[CrossRef](#)]
41. Yasin, S.A.; Abbas, J.A.; Ali, M.M.; Saeed, I.A.; Ahmed, I.H. Methylene blue photocatalytic degradation by TiO₂ nanoparticles supported on PET nanofibers. *Mater. Today Proc.* **2020**, *20*, 482–487. [[CrossRef](#)]
42. Nava, O.J.; Luque, P.A.; Gómez-Gutiérrez, C.M.; Vilchis-Nestor, A.R.; Castro-Beltrán, A.; Mota-González, M.L.; Olivas, A. Influence of Camellia sinensis extract on Zinc Oxide nanoparticle green synthesis. *J. Mol. Struct.* **2017**, *1134*, 121–125. [[CrossRef](#)]

43. Arumugam, M.; Murugesan, B.; Balasekar, P.; Malliappan, S.P.; Chinnalagu, D.K.; Chinniah, K.; Cai, Y.; Mahalingam, S. Silk fibroin and gelatin composite nanofiber combined with silver and gold nanoparticles for wound healing accelerated by reducing the inflammatory response. *Process Biochem.* **2023**, *134*, 1–16. [[CrossRef](#)]
44. Salleh, M.A.M.; Mahmoud, D.K.; Karim, W.A.W.A.; Idris, A. Cationic and anionic dye adsorption by agricultural solid wastes: A comprehensive review. *Desalination* **2011**, *280*, 1–13. [[CrossRef](#)]
45. Najim, T.S.; Yassin, S.A.; Dawood, B.A. Synthesis of Peppermint stem-g-Poly (acrylic acid) and its application for Nickel ions removal. *Iraqi J. Polym.* **2012**, *16*, 34–46.
46. Joshi, S.; Garg, V.K.; Kataria, N.; Kadirvelu, K. Applications of Fe₃O₄@ AC nanoparticles for dye removal from simulated wastewater. *Chemosphere* **2019**, *236*, 124280. [[CrossRef](#)]
47. Agarwal, S.; Tyagi, I.; Gupta, V.K.; Ghasemi, N.; Shahivand, M.; Ghasemi, M. Kinetics, equilibrium studies and thermodynamics of methylene blue adsorption on Ephedra strobilacea saw dust and modified using phosphoric acid and zinc chloride. *J. Mol. Liq.* **2016**, *218*, 208–218. [[CrossRef](#)]
48. Nasrullah, A.; Khan, H.; Khan, A.S.; Man, Z.; Muhammad, N.; Khan, M.I.; El-Salam, A.; Naser, M. Potential biosorbent derived from Calligonum polygonoides for removal of methylene blue dye from aqueous solution. *Sci. World J.* **2015**, *2015*, 562693. [[CrossRef](#)] [[PubMed](#)]
49. Abdullah, A.H.; Yasin, S.A.; Abdullah, S.M.; Khalaf, M.Y.; Saeed, I.A. A kinetic and isotherm study on removing methylene blue from aqueous solutions by oxidized cellulose nanostructure. *Emergent Mater.* **2022**, *5*, 1199–1212. [[CrossRef](#)]
50. Kumar, P.S.; Ramalingam, S.; Senthamarai, C.; Niranjana, M.; Vijayalakshmi, P.; Sivanesan, S. Adsorption of dye from aqueous solution by cashew nut shell: Studies on equilibrium isotherm, kinetics and thermodynamics of interactions. *Desalination* **2010**, *261*, 52–60. [[CrossRef](#)]
51. Totito, T.C.; Laatikainen, K.; Perea, O.; Bode-Aluko, C.; Petrik, L. Adsorptive recovery of Cu²⁺ from aqueous solution by polyethylene terephthalate nanofibres modified with 2-(aminomethyl) pyridine. *Appl. Sci.* **2021**, *11*, 11912. [[CrossRef](#)]
52. Wang, J.; Guo, X. Adsorption kinetic models: Physical meanings, applications, and solving methods. *J. Hazard. Mater.* **2020**, *390*, 122156. [[CrossRef](#)]
53. Islam, M.S.; McPhedran, K.N.; Messele, S.A.; Liu, Y.; El-Din, M.G. Isotherm and kinetic studies on adsorption of oil sands process-affected water organic compounds using granular activated carbon. *Chemosphere* **2018**, *202*, 716–725. [[CrossRef](#)] [[PubMed](#)]
54. Rakass, S.; Hassani, H.O.; Mohmoud, A.; Kooli, F.; Abboudi, M.; Assirey, E.; Al Wadaani, F. Highly efficient methylene blue dye removal by nickel molybdate nanosorbent. *Molecules* **2021**, *26*, 1378. [[CrossRef](#)] [[PubMed](#)]
55. Elmorsi, T.M. Equilibrium isotherms and kinetic studies of removal of methylene blue dye by adsorption onto miswak leaves as a natural adsorbent. *J. Environ. Prot.* **2011**, *2*, 817. [[CrossRef](#)]
56. El-Ghobashy, M.A.; Salem, I.A.; El-Dahrawy, W.M.; Salem, M.A. Fabrication of α -MnO₂/Fe-Mn binary oxide nanocomposite as an efficient adsorbent for the removal of methylene blue from wastewater. *J. Mol. Struct.* **2023**, *1272*, 134118. [[CrossRef](#)]
57. Hasani, N.; Selimi, T.; Mele, A.; Thaçi, V.; Halili, J.; Berisha, A.; Sadiku, M. Theoretical, equilibrium, kinetics and thermodynamic investigations of methylene blue adsorption onto lignite coal. *Molecules* **2022**, *27*, 1856. [[CrossRef](#)]
58. Pathania, D.; Sharma, S.; Singh, P. Removal of methylene blue by adsorption onto activated carbon developed from Ficus carica bast. *Arab. J. Chem.* **2017**, *10*, S1445–S1451. [[CrossRef](#)]
59. El Gaayda, J.; Titchou, F.E.; Oukhrif, R.; Karmal, I.; Oualid, H.A.; Berisha, A.; Zazou, H.; Swanson, C.; Hamdani, M.; Akbour, R.A. Removal of cationic dye from coloured water by adsorption onto hematite-humic acid composite: Experimental and theoretical studies. *Sep. Purif. Technol.* **2022**, *288*, 120607. [[CrossRef](#)]
60. Deivasigamani, P.; Kumar, P.S.; Sundaraman, S.; Soosai, M.R.; Renita, A.A.; Karthikeyan, M.; Bektenov, N.; Baigenzhenov, O.; Venkatesan, D.; Kumar, A. Deep insights into kinetics, optimization and thermodynamic estimates of methylene blue adsorption from aqueous solution onto coffee husk (*Coffea arabica*) activated carbon. *Environ. Res.* **2023**, *236*, 116735. [[CrossRef](#)]
61. Murugesan, A.; Divakaran, M.; Raveendran, P.; Nikamanth, A.B.N.; Thelley, K.J. An eco-friendly porous poly (imide-ether) s for the efficient removal of methylene blue: Adsorption kinetics, isotherm, thermodynamics and reuse performances. *J. Polym. Environ.* **2019**, *27*, 1007–1024. [[CrossRef](#)]
62. Fito, J.; Abewaa, M.; Mengistu, A.; Angassa, K.; Ambaye, A.D.; Moyo, W.; Nkambule, T. Adsorption of methylene blue from textile industrial wastewater using activated carbon developed from Rumex abyssinicus plant. *Sci. Rep.* **2023**, *13*, 5427. [[CrossRef](#)]
63. Sadek, A.H.; Mostafa, M.K. Preparation of nano zero-valent aluminum for one-step removal of methylene blue from aqueous solutions: Cost analysis for scaling-up and artificial intelligence. *Appl. Water Sci.* **2023**, *13*, 34. [[CrossRef](#)]
64. Hassan, A.F.; El-Naggar, G.A.; Esmail, G.; Shaltout, W.A. Efficient adsorption of methylene blue on novel triple-nanocomposites of potassium Kappa-carrageenan, calcium alginate and nanohydroxyapatite obtained from sea scallop shells. *Appl. Surf. Sci. Adv.* **2023**, *13*, 100388. [[CrossRef](#)]
65. Handayani, T.; Ramadhani, P.; Zein, R. Modelling studies of methylene blue dye removal using activated corn husk waste: Isotherm, kinetic and thermodynamic evaluation. *S. Afr. J. Chem. Eng.* **2024**, *47*, 15–27. [[CrossRef](#)]
66. Shao, Y.; Zhou, L.; Bao, C.; Ma, J.; Liu, M.; Wang, F. Magnetic responsive metal-organic frameworks nanosphere with core-shell structure for highly efficient removal of methylene blue. *Chem. Eng. J.* **2016**, *283*, 1127–1136. [[CrossRef](#)]

67. Mansour, A.T.; Alprol, A.E.; Abualnaja, K.M.; El-Beltagi, H.S.; Ramadan, K.M.A.; Ashour, M. The Using of Nanoparticles of Microalgae in Remediation of Toxic Dye from Industrial Wastewater: Kinetic and Isotherm Studies. *Materials* **2022**, *15*, 3922. [[CrossRef](#)]
68. Shi, Y.; Chang, Q.; Zhang, T.; Song, G.; Sun, Y.; Ding, G. A review on selective dye adsorption by different mechanisms. *J. Environ. Chem. Eng.* **2022**, *10*, 108639. [[CrossRef](#)]

Disclaimer/Publisher's Note: The statements, opinions and data contained in all publications are solely those of the individual author(s) and contributor(s) and not of MDPI and/or the editor(s). MDPI and/or the editor(s) disclaim responsibility for any injury to people or property resulting from any ideas, methods, instructions or products referred to in the content.